The mechanics of clay smearing along faults

D.L. Egholm[1], O.R. Clausen[1], M. Sandiford[2], M.B. Kristensen[3], J.A. Korstgård[1]
[1]Department of Earth Sciences, University of Aarhus, Nordre Ringgade 1, DK-8000 Aarhus C, Denmark
[2]School of Earth Sciences, University of Melbourne, Melbourne, Victoria 3010, Australia
[3]Shell UK Exploration and Production, 1 Altens Farm Road, Nigg, Aberdeen, Grampian AB12 3FY, UK

ABSTRACT

A clay- or shale-rich fault gouge can significantly reduce fault permeability. Therefore, predictions of the volume of clay or shale that may be smeared along a fault trace are important for estimating the fluid connectivity of groundwater and hydrocarbon reservoir systems. Here, we show how fault smears develop spontaneously in layered soil systems with varying friction coefficients, and we present a quantitative dynamic model for such behavior. The model is based on Mohr-Coulomb failure theory, and using discrete element computations, we demonstrate how the model framework can predict the fault smear potential from soil friction angles and layer thicknesses.

Keywords: clay smear, faults, soft-sediment deformation, Mohr-Coulomb.

INTRODUCTION

Smearing of low-permeability clay is one of the most important conditions promoting fault sealing (e.g., Caine et al., 1996), and so assessment of fault smear distribution is of key importance for evaluating the fluid connectivity of hydrocarbon reservoirs and groundwater systems alike. An important new and urgent impetus for improved understanding of the sealing potential of subsurface reservoirs is provided by issue of sequestration of CO_2 (e.g., Bickle et al., 2007).

The mechanical prerequisites for development of clay smear remain, however, poorly known. Outcrop field studies (Fig. 1) (Lindsay et al., 1993; Lehner and Pilaar, 1997; Bense et al., 2003; van der Zee and Urai, 2005) and laboratory experiments (Sperrevik et al., 2000; Clausen and Gabrielsen, 2002) indicate that clay smear develops from a combination of clay intrusion from source layers, and from shearing within the fault zone. A key observation shows that clay smears range from 10^{-2} to 10^{2} m, forming continuous bands that connect but gradually thin away from faulted source beds. Smear thickness correlates to source bed thickness and the competence contrast between layers. Thick and weak source beds produce the thickest smears and hence best fault seals (Lehner and Pilaar, 1997; Clausen and Gabrielsen, 2002).

Predictive assessment of fault sealing by clay smearing at depth in prospective reservoirs therefore requires a priori knowledge about the fault throw as well as relative thicknesses of the source clay layers that provide material for the smear and the intervening layers that need sealing. The clay smear potential (CSP) (Fulljames et al., 1997) represents one of several semi-empirical relations that have yielded some success (e.g., Yielding et al., 1997), although they suffer from a lack of physical basis by relating predicted fault smear thickness to geometric properties only, and not to the mechanical properties of clay and sand. The CSP model estimates the sealing capacity of clay smears as:

$$\mathrm{CSP} = \mathrm{c}\frac{T_c^2}{d}, \quad (1)$$

where T_c is the thickness of the clay source bed, d is the distance from the source bed, and c is a constant that needs to be calibrated.

Here, we use Mohr-Coulomb theory to show how smearing is a natural consequence of fault-related deformation of layered granular material with differing friction coefficients, such as clay and sand, and we demonstrate how Mohr-Coulomb theory provides a simple predictive framework for assessing clay smear fault seals, much like the CSP model above, but including the effect of material properties. Our model approach does not include all elements that may possibly influence the clay smearing process. In particular, viscous-rate effects and pore-pressure variations are ignored. On the other hand, our simplistic model illustrates the full effect of a common and basic assumption of a competence contrast between clay and sand, and it demonstrates how this assumption is sufficient in promoting clay smears, thereby providing a useful predictive framework for seal assessment.

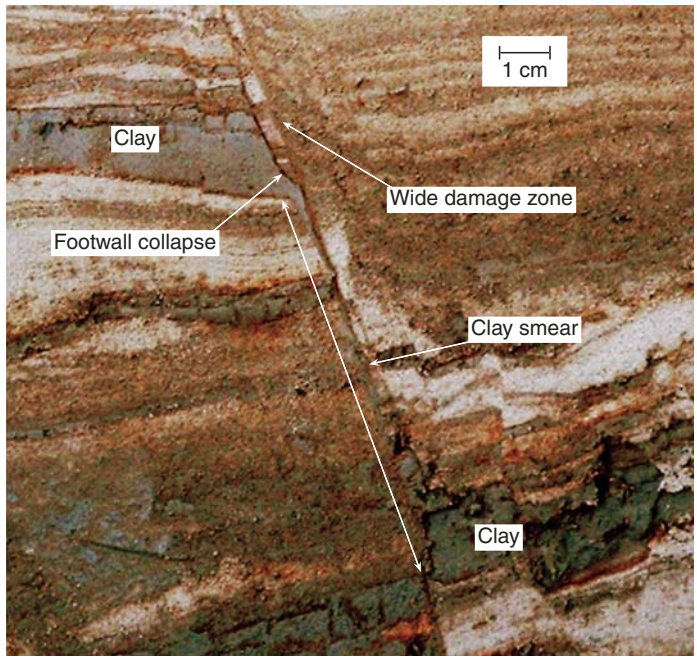

Figure 1. Outcrop from Nr. Lyngby, Denmark. Sediments exposed are late to postglacial deposits of sand, silt, and clay. Relatively thick clay layer is offset by a steep normal fault, and between footwall and hanging-wall parts of source layer, a smear has developed. Footwall part of clay layer is partially collapsed, and wider damage zone has developed in sand above.

A MOHR-COULOMB FRAMEWORK

The Mohr-Coulomb criterion for failure of granular material relates the failure plane shear stress, σ_s, to normal stress, σ_n:

$$\sigma_s = \tan(\varphi)\sigma_n + c, \quad (2)$$

where φ is the angle of internal friction and c is cohesion. For any critical stress precisely satisfying the Mohr-Coulomb criterion, shear failure occurs on planes parallel to the failure plane angle (Mandl, 2000) (Fig. 2D):

$$\theta = 45° + \varphi/2. \quad (3)$$

Generally, φ > 30° in sands, and consequently, for normal faults (where σ_3 is horizontal), θ > 60°. Shale and clay generally have smaller friction angles than sands (e.g., Wood, 1990). Thus, under conditions of normal faulting, failure plane angles of sand and shale differ by as much as 25°, particularly when bedding-induced fabric is considered (Arch et al., 1988).

According to Mohr-Coulomb theory, a fault intersecting a bed of lower friction angle will refract to a shallower orientation with respect to σ_3, creating a "contractional" bend. Movement on a surface with a contractional bend leads to an increase in mean stress along the fault plane within the low-friction-angle material, and a decrease in the high-friction-angle material. For the case of a layered clay-sand package, stress gradients produced by progressive fault slip will promote granular flow of the clay into the low-mean-stress fault segments between bridging sands. Because of the requirement for flow along failure planes set by the internal angle of friction, material flow is restricted to the limited zone (Fig. 2D) of instability in the clay layers, demarcating the volume, V, of potential smearing clay:

$$V = \left[\cot(\theta_c) - \cot(\theta_s)\right] T_c^2, \quad (4)$$

where T_c is the thickness of the clay layer, and θ_c and θ_s are the failure plane angles of clay and sand. Material flow within this zone of instability refracts the effective fault trace, thereby facilitating the development of the "contractional bend" (Childs et al., 1996).

If we assume that clay smear thickness scales with the volume of unstable clay divided by the total length of the fault trace, L_f (Fig. 2D), we get:

$$\overline{T}_{cs} \propto \frac{V}{L_f} = \left[\cot(\theta_c) - \cot(\theta_s)\right] \frac{T_c^2}{L_f} \quad (5)$$

as a model for the average clay smear thickness, $\overline{T}_{cs}$. The latter T_c^2/L_f dependency resembles the CSP model (Fulljames et al., 1997), whereas the dependency of θ_c and θ_s in Equation 5 introduces the rheological control the CSP model lacks.

COMPUTATIONAL MODELING

In order to gain further insight into how smears develop within the Mohr-Coulomb framework and assess whether Equation 5 provides a useful predictive basis for clay smear development, we performed computer simulations based on the stress-based discrete element method (SDEM; Egholm, 2007; Egholm et al., 2007). SDEM is an extension of the better known discrete element method (Cundall and Strack, 1979) or molecular dynamics method (Allen and Tildesley, 1987). All three methods are free of mesh structures, as the granular matter is represented by discrete spherical particles, permitting large and localized deformations. The particles interact mechanically by normal and shear contact forces. Importantly, SDEM regulates particle behavior directly in terms of the macrophysical Mohr-Coulomb parameters and thus differs from the original DEM formulation, which requires these parameters to be set by "experimental" calibration of microphysical contact properties. The SDEM parameterization is therefore better suited for simulations where rules governing the microphysical grain interactions are poorly known, and where instead the macroscopic Mohr-Coulomb failure model is the preferred conceptual model for understanding frictional-cohesive brittle failure and flow.

Our model setup is illustrated by Figure 2A. A 60-cm-long and 30-cm-high, two-dimensional box was filled with 120,000 particles of random radii between 0.2 and 2.0 mm and with density 3.0 g/cm^3. The particles settled under gravity until static conditions were achieved. During settling, all particles were assigned a low friction angle (φ = 5°) and zero cohesion, resulting in uniform compaction with average porosity of 31%. The random particle-size distribution ensured irregular packing without geometric anisotropy, which could introduce unphysical constraints on the failure plane orientation. The particle size variation did not represent the effect of real grain-size variations. Instead, grain size was considered to be one of the microparameters effectively controlling the angle of internal friction. After settling, the middle 10 cm layer of particles was assigned a low friction angle, φ_c = 5°, representing clay, while both top and bottom layers were assigned a higher friction angle, φ_s = 35°, thereby representing sand. All particles were given cohesion of 100 Pa, resembling poorly lithified sediments. The model sides were frictionless, while the model base had the friction properties of sand.

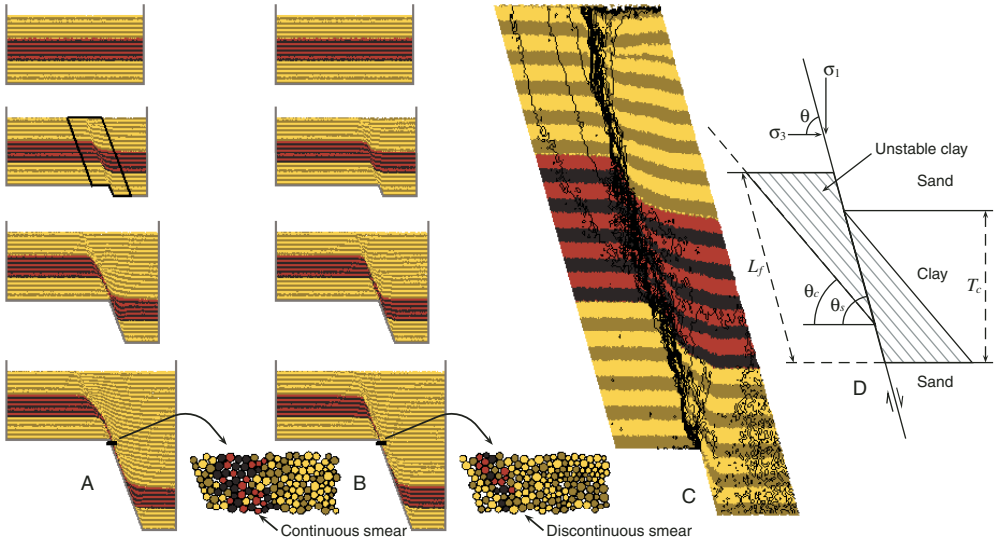

Figure 2. Evolution of two computational stress-based discrete element method (SDEM) models: (A) with clay layer (red) and (B) without clay layer (red layer in B is colored for easy comparison only). Model A has continuous and thick smear even at >40 cm of fault offset, while in pure sand model, red layer is breached at large offset. Enlarged insets to right of each bottom panel in A and B show individual SDEM particles in small area of fault zone. (C) Enlarged view (see polygon in second row of part A) of fault zone after 5 cm of fault slip with contours of particle speed. (D) Sketch showing how destabilization of clay around fault zone is predicted from Mohr-Coulomb failure theory.

The layered model particles were then activated by moving the right part of the model base and the right model side downward in a 65° direction with a speed of 1 cm/s, simulating an active "basement fault" and forcing a shear zone to propagate quasi-statically upward through the model domain. This kinematic boundary condition delivers a simple and general structural framework for fault propagation, although it represents just one of several possible kinematic situations. On the hanging-wall side, new particles were continuously added to simulate sedimentation and to prevent a surface slope from developing.

The model evolution is shown in Figure 2A at four stages corresponding to 0, 5, 20, and 42 cm of basement fault throw. The red and yellow layers are clay and sand, respectively. Both clay and sand layers are streaked by darker colors to visualize internal deformation. Figure 2B shows the corresponding progression of a pure sand reference model (the middle layer is colored for easy comparison only) at the same four stages. A comparison of the two models reveals the effect of the lower clay friction angle, as this represents the only difference in initial conditions of the models.

In both situations, a band of red particles is formed in the fault zone by shearing. However, after 25 cm of fault slip, the band is breached in Figure 2B, where the red layer is sand, while in Figure 2A, where the red layer is clay, the band remains continuous. The difference is explained by flow of clay into the fault zone. In Figure 2A, the footwall part of the source layer adjacent to the fault zone thins as particles flow along shallower failure planes into the fault zone. The latter effect is further illustrated in Figure 2C, which is an enlarged view of the fault zone after 5 cm of fault slip, and where contours of particle speed are shown. In the top and bottom sand layers, contours are concentrated in the fault zone, signaling intense and localized shearing. In the clay layer, contours are distributed in a wider zone delimited by the preferred clay failure planes (Fig. 2D). In the footwall part, the shallower clay failure planes connect to the surface along steeper failure planes in the sand layer above, which in turn is responsible for secondary faults developing in the sand above the unstable clay layer.

Figure 3 illustrates the fault-zone evolution in five stages from 0.1 to 42 cm offset. In the initial phase, deformation in the lower sand layer is governed by a near-vertical "precursor" fault (Mandl, 2000; Adam et al., 2005), which rotates to a shallower orientation in the clay layer. As the offset increases (10 cm), the deformation band steepens in the clay, forming a kinematically more favorable straight fault zone. With further displacement, the fault zone widens as clay moves down the fault. Figure 3B shows how clay is pressurized by the shear movement of the fault, while the sand pressure is relaxed as expected in a fault with a contractional bend (Childs et al., 1996).

To test the sensitivity of the smear mechanism, we modeled scenarios with varying clay friction angle (φ_c and clay layer thickness (T_c) and measured the average smear thickness ($\overline{T}_{cs}$) after fault slip of 42 cm. The results are presented in Figures 4A and 4B, where each open circle represents the result of one model. The solid lines are predictions based on Equation 5. Overall, we find the computational models confirm Equation 5. Figure 4C shows the smear thickness as a function of the normalized distance from the source bed (d/L_f) down along the fault for the model with $\varphi_c = 5°$ and offset of 42 cm. The model resolution clearly limits the internal structure of the model shear zone. However, the smear thickness is seen to decrease and attain a minimum halfway, $d/L_f = 0.5$, between the footwall and hanging-wall source layers. This is in agreement with existing models for clay smear potential (CSP) (Fulljames et al., 1997) assuming a $1/d$ relation between smear thickness and distance along the fault trace. For comparison, the CSP model is plotted as a solid line in Figure 4C.

DISCUSSION

The SDEM modeling provides new insights into the mechanics of clay smearing that can be compared with previous interpretations. For example, Lehner and Pilaar (1997) suggested that fault smearing relates to "pull-apart" kinematics, offsetting the normal fault across the shale beds and forming an extensional releasing bend (Peacock and Zhang, 1994; Childs et al., 1996). According to Lehner and Pilaar (1997), the releasing bend is required for (1) generating the horizontal stress relief, which is in turn responsible for driving the clay into the fault zone, and (2) for creating space for the clay material in the fault zone. Using a computational model, van der Zee et al. (2003) confirmed that a releasing bend does lead to clay injection into the fault zone. However, the releasing bend was imposed as an initial condition, and its genesis and relation to material properties are therefore not addressed.

As we have shown for Mohr-Coulomb materials, extensional bends are expected where faults intersect materials with relatively high friction angles, and contractional bends are likely where faults intersect clay layers embedded within sand layers. In the Mohr-Coulomb framework, along the contractional bend, clay is destabilized, and increased pressure caused by the movement of the steeper fault zone promotes the flow of unstable clay into the dilating fault zone in bridging sands. In essence, the driving force behind the evolution of the pressure field in the evolving fault system is provided by the progressive partitioning of gravitational stresses onto the contractional bend segments within low-frictional-angle materials. In addition to providing the driving force for

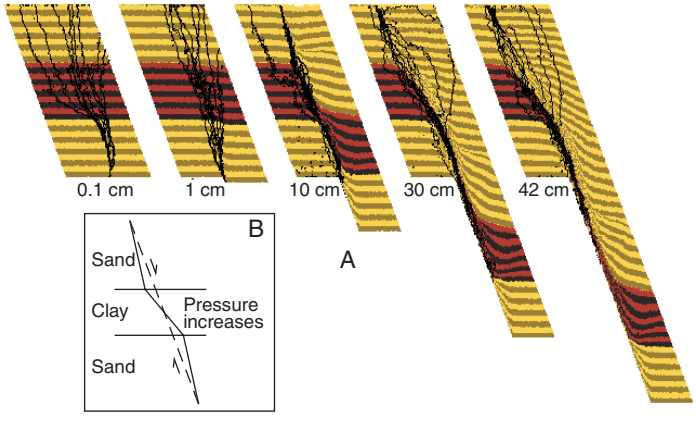

Figure 3. (A) Fault-zone evolution as offset increases. Area shown is indicated by black polygon in Figure 2A. Contours are of particle speed. (B) Increasing clay pressure in fault zone while sand parts dilate.

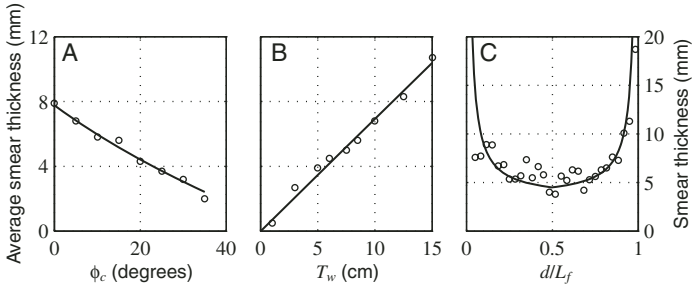

Figure 4. Clay smear thickness averaged along fault trace and measured after 42 cm of fault slip, for models with varying (A) clay friction angle and (B) clay layer thickness. Open circles are computational model results, while solid lines are based on Equation 5. A and B share vertical axis. (C) Smear thickness (open circles) measured as function of normalized distance, d/L_f, down along fault trace for model with $\varphi_c = 5°$. Solid line is clay smear potential (CSP) model of Fulljames et al. (1997).

fault smearing, contractional bends lead naturally to secondary faults in the footwall and hanging-wall sand layers that are ~0.5–1× the clay bed's thickness away from the main fault (Fig. 2C). These secondary faults effectively widen the fault damage zone in the sand, as observed in many natural examples (Heynekamp et al., 1999; Bense et al., 2003; van der Zee and Urai, 2005; Bense and Person, 2006).

However, still within the Mohr-Coulomb model framework, if clay beds are sufficiently cohesive, near-vertical tensile joints may initially steepen the fault trace across the clay bed, thereby generating an extensional bend in accordance with the "pull-apart" model of Lehner and Pilaar (1997). In this case, however, if the cohesive clay fails, it still slides along lower dipping planes (due to the low friction angle), and Equation 5 is still valid, although the clay now destabilizes in lumps and flows into the fault zone as a wedge-shaped larger mass before it is sheared and distributed along the fault (Sperrevik et al., 2000; Clausen and Gabrielsen, 2002).

An important limitation of the Mohr-Coulomb framework is that it is essentially rate independent, providing no platform for evaluating the importance of fault-slip rates. While clays are known to show some rate dependency, experimental studies reveal no consistent dependence on deformation rate (Sperrevik et al., 2000; Clausen and Gabrielsen, 2002), and it is unclear what it means for the smear potential. However, computationally, a visco-plastic clay rheology was addressed recently by Gudehus and Karcher (2007), who noted a clear asymptotic behavior of the smear thickness versus fault-offset curve. We also note here that a pure viscous end-member rheology for clay resembles a purely cohesive, but rate-dependent, strength proxy with an effective friction angle of zero, which would likely enhance the smear potential at low deformation rates.

Water content variations induced by compaction also affect the strength of clays and thus must influence smear potential. On the basis of triaxial tests, Arch et al. (1988) concluded that clay cohesion increases with decreasing water content. However, the friction angle was observed to decrease with decreasing water content, as the anisotropic effect of the bedding-parallel fabric intensifies. In contrast, ring-shear experiments (Clausen and Gabrielsen, 2002) have revealed how high levels of normal stress (200–500 kPa), and hence low water content, generally favor clay smearing. Thus, the way in which fault smearing potential varies with burial remains an open question requiring, for example, better characterization of Mohr-Coulomb properties.

In summary, fault smearing in layered sand and shale/clay sequences can be explained using Mohr-Coulomb failure theory, where contrasts in friction angles lead to triangular-shaped areas of instability in source layers. Computational models indicate that smear thickness scales with the area of the unstable triangle, which in turn is a simple function (Equation 5) of source bed thickness and friction angle contrast.

ACKNOWLEDGMENTS

We thank Graham Yielding, Janos Urai, and Victor Bense for constructive reviews that greatly improved the manuscript. The study was supported by the Carlsberg Foundation and the Danish Independent Research Council.

REFERENCES CITED

Adam, J., Urai, J.L., Wieneke, B., Oncken, O., Pfeiffer, K., Kukowski, N., Lohrmann, J., Hoth, S., van der Zee, W., and Schmatz, J., 2005, Shear localisation and strain distribution during tectonic faulting—New insights from granular-flow experiments and high-resolution optical image correlation techniques: Journal of Structural Geology, v. 27, p. 283–301, doi: 10.1016/j.jsg.2004.08.008.

Allen, M., and Tildesley, D., 1987, Computer Simulations of Liquids: New York, Oxford University Press, 408 p.

Arch, J., Maltman, A.J., and Knipe, R.J., 1988, Shear-zone geometries in experimentally deformed clays: The influence of water content, strain rate and primary fabric: Journal of Structural Geology, v. 10, p. 91–99, doi: 10.1016/0191–8141(88)90131–9.

Bense, V., and Person, M.A., 2006, Faults as conduit-barrier systems to fluid flow in siliciclastic sedimentary aquifers: Water Resources Research, v. 42, p. w05421, doi: 10.1029/2005WR004480.

Bense, V., Van den Berg, E., and Van Balen, R., 2003, Deformation mechanisms and hydraulic properties of fault zones in unconsolidated sediments; the Roer Valley Rift System, The Netherlands: Hydrogeology Journal, v. 11, p. 319–332.

Bickle, M., Chadwick, A., Huppert, H.E., Hallworth, M., and Lyle, S., 2007, Modelling carbon dioxide accumulation at Sleipner: Implications for underground carbon storage: Earth and Planetary Science Letters, v. 255, p. 164–176, doi: 10.1016/j.epsl.2006.12.013.

Caine, J.S., Evans, J.P., and Forster, C.B., 1996, Fault zone architecture and permeability structure: Geology, v. 24, no. 11, p. 1025–1028, doi: 10.1130/0091–7613(1996)024<1025:FZAAPS>2.3.CO;2.

Childs, C., Nicol, A., Walsh, J.J., and Watterson, J., 1996, Growth of vertically segmented normal faults: Journal of Structural Geology, v. 18, no. 12, p. 1389–1397, doi: 10.1016/S0191–8141(96)00060–0.

Clausen, J., and Gabrielsen, R., 2002, Parameters that control the development of clay smear at low stress states: An experimental study using ring-shear apparatus: Journal of Structural Geology, v. 24, p. 1569–1586, doi: 10.1016/S0191–8141(01)00157–2.

Cundall, P., and Strack, O., 1979, A discrete numerical model for granular assemblies: Geotechnique, v. 29, p. 47–65.

Egholm, D.L., 2007, A new strategy for discrete element numerical models: Part I: Theory: Journal of Geophysical Research, v. 112, B05203, doi: 10.1029/2006JB004557.

Egholm, D.L., Sandiford, M., Clausen, O.R., and Nielsen, S.B., 2007, A new strategy for discrete element numerical models. Part II: Applications: Journal of Geophysical Research, v. 112, B05204, doi: 10.1029/2006JB004558.

Fulljames, J.R., Zijerveld, L.J.J., and Franssen, R.C.M.W., 1997, Fault seal processes: Systematic analysis of fault seals over geological and production time scales, *in* Møller-Pedersen, P., and Koestler, A.G., eds., Hydrocarbon Seals: Importance for Exploration and Production: Norwegian Petroleum Society Special Publication 7, p. 51–59.

Gudehus, G., and Karcher, C., 2007, Hypoplastic simulation of normal faults without and with clay smears: Journal of Structural Geology, v. 29, no. 3, p. 530–540, doi: 10.1016/j.jsg.2006.09.011.

Heynekamp, M.R., Goodwin, L.B., Mozley, P.S., and Haneberg, W.C., 1999, Controls on fault zone architecture in poorly lithified sediments, Rio Grande Rift, New Mexico: Implications for fault-zone permeability and fluid flow, *in* Haneberg, W.C., Mozley, P.S., Moore, J.C., and Goodwin, L.B., eds., Faults and Subsurface Fluid Flow in the Shallow Crust: American Geophysical Union Geophysical Monograph 113, p. 27–49.

Lehner, F.K., and Pilaar, W.F., 1997, The emplacement of clay smears in synsedimentary normal faults: Inferences from field observations near Frechen, Germany, *in* Møller-Pedersen, P., and Koestler, A.G., eds., Hydrocarbon Seals: Importance for Exploration and Production: Norwegian Petroleum Society Special Publication 7, p. 39–50.

Lindsay, N., Murphy, F., Walch, J., and Watterson, J., 1993, Outcrop studies of shale smears on fault surfaces, *in* Flint, S., and Bryant, I., eds., The Geological Modelling of Hydrocarbon Reservoirs and Outcrop Analogs: International Association of Sedimentologists Special Publication 15, p. 113–123.

Mandl, G., 2000, Faulting in Brittle Rocks. An Introduction to the Mechanics of Tectonic Faults: Berlin, Springer-Verlag, 436 p.

Peacock, D.C.P., and Zhang, X., 1994, Field examples and numerical modelling of oversteps and bends along normal faults in cross section: Tectonophysics, v. 234, p. 147–167, doi: 10.1016/0040–1951(94)90209–7.

Sperrevik, S., Færseth, R., and Gabrielsen, R., 2000, Experiments on clay smear formation along faults: Petroleum Geoscience, v. 6, p. 113–123.

van der Zee, W., and Urai, J.L., 2005, Processes of normal fault evolution in a siliciclastic sequence: A case study from Miri, Sarawak, Malaysia: Journal of Structural Geology, v. 27, p. 2281–2300, doi: 10.1016/j.jsg.2005.07.006.

van der Zee, W., Urai, J.L., and Richard, P.D., 2003, Lateral clay injection into normal faults: GeoArabia, v. 8, p. 501–522.

Wood, D.W., 1990, Soil Behaviour and Critical Soil Mechanics: New York, Cambridge University Press, 486 p.

Yielding, G., Freeman, B., and Needham, D., 1997, Quantitative fault seal prediction: American Association of Petroleum Geologists (AAPG) Bulletin, v. 81, p. 897–917.

Manuscript received 20 March 2008
Revised manuscript received 12 June 2008
Manuscript accepted 23 June 2008

Printed in USA